Conformal invariance, multifractality, and finite-size scaling at Anderson localization transitions in two dimensions

H. Obuse,[1,2,3] A. R. Subramaniam,[3,*] A. Furusaki,[1] I. A. Gruzberg,[3] and A. W. W. Ludwig[4]
[1]*Condensed Matter Theory Laboratory, RIKEN, Wako, Saitama 351-0198, Japan*
[2]*Department of Physics, Kyoto University, 060-8502 Kyoto, Japan*
[3]*James Franck Institute, University of Chicago, 5640 South Ellis Avenue, Chicago, Illinois 60637, USA*
[4]*Department of Physics, University of California, Santa Barbara, California 93106, USA*
(Received 2 December 2009; revised manuscript received 9 April 2010; published 19 July 2010)

We generalize universal relations between the multifractal exponent α_0 for the scaling of the typical wave-function magnitude at a (Anderson) localization-delocalization transition in two dimensions and the corresponding critical finite-size-scaling (FSS) amplitude Λ_c of the typical localization length in quasi-one-dimensional (Q1D) geometry: (i) when *open* boundary conditions are imposed in the transverse direction of Q1D samples (strip geometry), we show that the corresponding critical FSS amplitude Λ_c^o is universally related to the *boundary* multifractal exponent α_0^s for the typical wave-function amplitude along a straight boundary (surface). (ii) We further propose a generalization of these universal relations to those symmetry classes whose density of states vanishes at the transition. (iii) We verify our generalized relations [Eqs. (6) and (7)] numerically for the following four types of two-dimensional Anderson transitions: (a) the metal-to-(ordinary insulator) transition in the spin-orbit (symplectic) symmetry class, (b) the metal-to-($\mathbb{Z}_2$ topological insulator) transition which is also in the spin-orbit (symplectic) class, (c) the integer quantum-Hall plateau transition, and (d) the spin quantum-Hall plateau transition.

DOI: 10.1103/PhysRevB.82.035309 PACS number(s): 73.20.Fz, 05.45.Df, 72.15.Rn

I. INTRODUCTION

Localization-delocalization (LD) or Anderson localization transitions of noninteracting electrons are continuous phase transitions driven by disorder.[1–5] When disorder is weak, the single-electron wave functions are extended over the whole sample. Sufficiently strong disorder localizes electrons within a finite region in space. The linear size of this region is the localization length ξ characterizing the typical size of the wave functions $\psi(\boldsymbol{r})$.[1] As the disorder strength is reduced, the localization length increases and eventually diverges at an LD transition point. The localization length is the analogue of the correlation length at nonrandom continuous phase transitions. At the LD transition point, wave-function amplitudes obey scale-invariant, multifractal statistics;[6–9] that is, the disorder-averaged qth moment of the square of the absolute value of wave function has a power-law dependence on the linear dimension L of the system, with an exponent that is a nonlinear function of q.[5–7]

Let us recall that continuous phase transitions in *nonrandom* systems are known to be quite generally described by conformally invariant field theories. Conformal symmetry is especially powerful in two dimensions (2D), where its presence leads to an infinite number of symmetry constraints. This, in many cases, allows for a rather complete description of critical properties.[10,11] Effective (field) theories describing the *random* LD transitions are also expected to possess conformal symmetry. In fact, we have recently shown by numerical simulations of a standard LD transition occurring in two dimensions, namely, of the metal-insulator transition in the 2D spin-orbit (symplectic) symmetry class,[12] that multifractal exponents of critical wave functions evaluated on a straight boundary and those at a corner are related through a simple relation dictated by conformal symmetry.[13]

Conformal symmetry is known to impose strong constraints on finite-size scaling (FSS) for phase transitions in nonrandom systems with quasi-one-dimensional (Q1D) geometry. For these systems Cardy has shown[14] that the correlation length ξ which characterizes the decay of the two-point correlation function of any (conformal primary[10,15]) operator along a cylinder or a strip of width M, is related to the bulk (x_b) or surface (x_s) scaling dimension of the operator in two dimensions through

$$\frac{M}{\xi} = \begin{cases} 2\pi x_b, & \text{cylinder(periodic BC)}, \\ \pi x_s, & \text{strip(open BC)}. \end{cases} \tag{1}$$

Here BC stands for boundary conditions imposed in the transverse direction.

The generalization of Eq. (1) to scale-invariant disordered 2D systems was first provided in the study of random 2D diluted ferromagnets in Ref. 16 [for the 2D bulk exponents and Q1D cylinder geometry (periodic BCs)]. In a random system the scaling of an observable (such as, for example, a "spin") is in general characterized by the set of scaling dimensions x_q of all its qth moment disorder averages. Equation (1) generalizes[16] to all these moments. In particular, the correlation length ξ_q characterizing the exponential decay of the qth moment of a correlation function of the observable in Q1D cylinder geometry is related to the 2D scaling exponent by

$$\frac{M}{\xi_q} = 2\pi x_q, \quad \text{cylinder(periodic BC)}. \tag{2}$$

At the same time, by using an expansion about $q=0$ of the qth moments in the 2D system and in the Q1D cylinder geometry, it was demonstrated in Ref. 16 that such a relationship holds also for the corresponding "*typical*" quantities referring to a fixed disorder realization. In particular, if α_0 denotes the typical[16] 2D bulk scaling dimension of the observable, and if $1/\xi$ denotes the Lyapunov exponent characterizing the inverse of the typical Q1D correlation length in cylinder geometry, then again the relationship

$$\frac{M}{\xi} = 2\pi\alpha_0, \quad \text{cylinder(periodic BC)} \tag{3}$$

holds.

Later, Refs. 9 and 17 proposed a corresponding formula in the context of LD transitions in two dimensions,

$$\frac{M}{\xi_p} = 2\pi(\alpha_0^b - 2) \tag{4}$$

[the shift by two between the right-hand side of Eqs. (4) and (3) arises from different conventions]. Here, ξ_p is the typical Q1D localization length in *cylinder* geometry (the subscript p of ξ_p denotes periodic BCs imposed in the transverse direction). The exponent α_0^b in Eq. (4) characterizes the scaling of a typical critical wave-function amplitude in the *bulk* of a 2D system of linear dimension R,

$$\overline{\ln|\psi(\boldsymbol{r})|^2} \sim -\alpha_0^b \ln R, \tag{5}$$

where the overbar stands for the disorder average. Equation (4) has been confirmed numerically for the integer quantum-Hall (IQH) plateau transition[9,17,18] and for the 2D metal-insulator transition in the spin-orbit (symplectic) symmetry class.[13,19,20]

We note that the relation (4), in the form presented, is only valid for systems in which the average bulk density of states (DOS) is constant and nonvanishing at the transition. This is the case for LD transitions in the three Wigner-Dyson classes. These include the IQH plateau transition and the LD transition in the spin-orbit (symplectic) class. However, as is now well known, there are symmetry classes in which the DOS vanishes at the transition. This is the case, for example, for the so-called spin quantum-Hall transition of the Bogoliubov-de Gennes (BdG) quasiparticles in symmetry class C[21–23] (in the nomenclature of Ref. 25).

In this paper we derive a generalization of the relationship (4) between the exponent α_0^b and the typical Q1D correlation length ξ_p for LD transitions in 2D with a *vanishing* critical DOS. The result is

$$\frac{M}{\xi_p} = 2\pi(\alpha_0^b - 2 + x_\rho), \tag{6}$$

where the exponent x_ρ characterizes the critical behavior of the (bulk) DOS (x_ρ=0 in the Wigner-Dyson classes).

Furthermore, we derive a FSS formula for the typical Q1D localization length, when *open* BCs are imposed in the transverse direction. The specific open BC we consider in this paper is a reflecting BC which means that the system simply ends at the boundary so that there is no current flowing across the boundary. The second line of Eq. (1) suggests that the localization length should be related to a surface exponent characterizing multifractality of critical wave functions near boundaries of disordered systems.[24] Indeed, our result is the formula

$$\frac{M}{\xi_o} = \pi(\alpha_0^s - 2 + x_\rho), \tag{7}$$

where now α_0^s is the surface (i.e., boundary) exponent characterizing scaling of a typical wave-function amplitude near a straight (reflecting) boundary. α_0^s is defined in the same way as α_0^b in Eq. (5), except that now the point $\boldsymbol{r}$ is close to a straight boundary of the 2D system of linear dimension R. The typical Q1D localization length ξ_o is computed in the geometry of a strip of width M with open (reflecting) BCs imposed in the transverse direction (the subscript o stands for "open").

The organization of this paper is as follows. In Sec. II we derive Eqs. (6) and (7). In Sec. III we verify both these equations numerically by computing the critical FSS amplitude (Λ_p or Λ_o) of the typical Q1D localization length, defined as

$$\Lambda_p = \frac{2\xi_p}{M}, \quad \Lambda_o = \frac{2\xi_o}{M} \tag{8}$$

for both types of BCs (the factor 2 in this definition is standard convention). We verify Eq. (7) for (a) the metal-to-(ordinary) insulator transition in the spin-orbit (symplectic) class [class AII of Ref. 25], (b) the LD transition between a metal and a $\mathbb{Z}_2$ topological insulator in the "quantum spin-Hall" (QSH) effect[26] which also belongs to the spin-orbit (symplectic) class [class AII of Ref. 25], (c) the IQH plateau transition in the unitary symmetry class [class A of Ref. 25]. [The *bulk* relation, Eq. (6), was already verified for systems (a)–(c), where x_ρ=0, in previous work.[9,13,17–20]] We finally verify numerically Eqs. (6) and (7) for the spin quantum-Hall transition in symmetry class C of Ref. 25. Table I summarizes the numerical results presented in detail in Sec. III. Section IV presents our conclusions.

II. LOCALIZATION LENGTH AND MULTIFRACTALITY

In this section we provide a derivation of Eqs. (6) and (7). Let us begin with a brief discussion of the underlying assumptions. We are interested in scaling properties of the disorder average of some physical observable [e.g., the local DOS (LDOS)] at an LD transition point. One can recast this disorder average into a statistical average of a properly defined operator $\mathcal{O}$ in a certain field theory (e.g., a replica or supersymmetric nonlinear sigma model).[2,4] The scaling properties of $\mathcal{O}$ at the critical point are then controlled by the fixed point of the renormalization-group (RG) flow of the corresponding field theory. We are now ready to state the two important assumptions we make in our derivation:[27] (1) the fixed-point theory is a conformal field theory. (2) At the fixed point of the RG transformation, the operator $\mathcal{O}$ is a primary[10] field operator in the conformal field theory.

A. Finite-size scaling in cylinder geometry and bulk exponents

Let us consider a disordered electronic system at its critical point, confined to a disk of radius R in the 2D x-y plane, or equivalently, the complex plane with the coordinate z=x+iy. We assume that all along the boundary of the disk there

TABLE I. A list of α_0, x_ρ, and Λ_c for various universality classes. The values of α_0 marked by * are from the references listed in the last column. Those without * are obtained in this paper. The fifth column shows Λ_c calculated from α_0^b using Eq. (6) and from α_0^s using Eq. (7), combined with Eq. (8). These values of Λ_c should be compared with those obtained from fitting (as explained in Sec. III) and shown in the sixth column.

System	BCs	α_0	x_ρ	Λ_c from α_0	Λ_c from fit	Ref.
Symplectic (M-I)	Open	2.429 ± 0.006	0	1.48 ± 0.02	1.50 ± 0.01	This paper
Symplectic (M-QSH)	Open	$2.091 \pm 0.002^*$	0	7.00 ± 0.15	7.20 ± 0.01	Ref. 39
IQH	Open	2.385 ± 0.003	0	1.654 ± 0.013	1.624 ± 0.002	This paper
SQH in class C	Periodic	2.137^*	1/4	0.8225	0.8189 ± 0.0004	Ref. 48
SQH in class C	Open	2.326^*	1/4	1.105	1.101 ± 0.002	Ref. 24

is a metallic electrode attached, thus allowing for the electron in the system to escape.[28] This (absorbing) boundary condition introduces a finite broadening η of the single-particle levels in the system. We assume that the broadening is on the order of the mean level spacing in the system. This provides a regularization for Green's function and the LDOS as follows:

$$G_\pm(z,z';E) = \sum_n \frac{\psi_n^*(z)\psi_n(z')}{E - E_n \pm i\eta}, \tag{9}$$

$$\rho_E(z) = \frac{i}{2\pi}[G_+(z,z;E) - G_-(z,z;E)]$$
$$= \frac{1}{\pi}\sum_n |\psi_n(z)|^2 \frac{\eta}{(E-E_n)^2 + \eta^2}. \tag{10}$$

Here the wave functions $\psi_n(z)$ of the closed system are normalized in the disk: $\int_{|z|\le R}|\psi(z)|^2 d^2z = 1$. The integral of the LDOS $\rho_E(z)$ over the disk gives the global DOS ρ_E multiplied by the disk area πR^2.

Statistical properties of metallic or critical wave functions at energy E are closely related to those of the LDOS.[8] In particular, if we are interested in the scaling of the moments of such wave functions and the moments of the LDOS, we can write symbolically

$$|\psi_E(z)|^2 \sim \frac{\rho_E(z)}{\pi R^2 \rho_E}. \tag{11}$$

Disorder averages of powers of the LDOS $\rho_E(z)$ (as well as those of products of Green's function) are represented by expectation values of operators in the corresponding field theory.[2,4] We denote this by

$$\overline{[\rho_E(z)]^q} \sim \langle \mathcal{O}_q(z)\rangle, \tag{12}$$

where the angular brackets denote the expectation value in the field theory. Here $\mathcal{O}_q(z)$ is the operator which corresponds to the qth moment of $\rho_E(z)$. (We point out that here and in what follows the power q can take any real values.[29]) In view of Eq. (11), the same operator represents moments of the wave function $\psi_E(z)$,

$$(R^2\rho_E)^q \overline{|\psi_E(z)|^{2q}} \sim \langle \mathcal{O}_q(z)\rangle. \tag{13}$$

Notice that the global DOS is self-averaging and can be pulled out of the disorder average along with powers of the radius R. The product $R^2\rho_E \propto \delta^{-1}$, where δ is the mean level spacing in the disk.

Now we concentrate on the wave functions and the DOS *at the critical energy*, $E=E_c$, and drop the subscript E. The global DOS ρ may vanish at criticality in the infinite system. In a finite system the disorder-averaged ρ always has a power-law behavior,

$$\rho \sim R^{-x_\rho}, \tag{14}$$

where the exponent x_ρ vanishes in the standard Wigner-Dyson classes but is known to be nonzero in other symmetry classes. For example, at the (2D) spin quantum-Hall transition in symmetry class C,[21–23] the exact value is known, $x_\rho = 1/4$.[21]

We now make use of the previously stated assumptions[27] of conformal invariance and the fact that $\mathcal{O}_q$ is a primary[10] conformal scaling operator with the bulk scaling dimension x_q^b at the LD transition. If we choose a point $|z| \ll R$ close to the origin of the disk, then the one-point function (the field theory expectation value) scales as

$$\langle \mathcal{O}_q(z)\rangle \sim R^{-x_q^b}. \tag{15}$$

Combining this with Eqs. (13) and (14), we obtain the scaling of the moments of the critical wave functions,

$$\overline{|\psi(z)|^{2q}} \sim R^{-2q - x_q^b + q x_\rho} \tag{16}$$

for $|z| \ll R$. Notice that the exponent of R on the right-hand side should vanish at $q=0$, and should be -2 at $q=1$ due to the normalization of the wave function. These conditions determine

$$x_0^b = 0, \quad x_1^b = x_\rho. \tag{17}$$

Some important details of the definition and properties of multifractal exponents are in order here. A slightly more detailed[30] (coarse-grained) description of multifractal wave functions (in 2D) involves breaking the system into little square boxes B_i of size $r \times r$ labeled by i. The number of these boxes N scales as $N \sim (R/r)^2$. One then calculates the probability p_i for an electron to be in the ith box as

$$p_i = \int_{B_i} |\psi(z)|^2 d^2z \tag{18}$$

and forms the so-called average generalized inverse participation ratios,

$$\overline{P_q} = \sum_{i=1}^{N} \overline{p_i^q} = N\overline{p_i^q}. \tag{19}$$

(We have assumed that the system is homogeneous after disorder average.) Equation (16) implies the scaling relation

$$\overline{P_q} \sim \left(\frac{R}{r}\right)^{-\tau_q}, \quad \tau_q = 2(q-1) + x_q^b - qx_\rho, \tag{20}$$

where the set of exponents τ_q is usually referred to as the multifractal spectrum.

Note that the probabilities p_i whose moments enter the definition of $\overline{P_q}$ are bounded by $0 \le p_i \le 1$. This bound implies that $\overline{P_q}$ must be a nonincreasing function of q since $p_i^{q_1} \ge p_i^{q_2}$ for $q_1 < q_2$. Moreover since $p^q = \exp(q \ln p)$ is convex as a function of q, the same is true for $\overline{P_q}$. Then the multifractal spectrum τ_q in Eq. (20) must be a nondecreasing, concave function of q. Generally speaking, there may be a value of $q = q_f$ where τ_q has a horizontal tangent. Then it follows that $\tau_q = \text{const}$ for $q \ge q_f$. Such change in the behavior of τ_q from an increasing function to a constant is often referred to as "freezing" or "termination" (see Ref. 5 for more details). In all known cases the value q_f where such termination occurs satisfies $q_f > 0$. Then we can safely use Eq. (16), and similar equations in the following sections, in the vicinity of $q=0$ without worrying about a possible termination transition.

Expanding both sides of Eq. (16) in q about $q=0$ yields the typical scaling exponent, Eq. (5), where

$$\alpha_0^b = 2 - x_\rho + \left.\frac{dx_q^b}{dq}\right|_{q=0}. \tag{21}$$

Next, let us consider the conformal mapping

$$w = \frac{M}{2\pi}\ln z, \quad z = \exp\left(\frac{2\pi}{M}w\right), \tag{22}$$

which maps the disk to the semi-infinite cylinder of circumference M in the complex w plane,

$$w = u + iv, \quad u \le L \equiv \frac{M}{2\pi}\ln R, \quad 0 \le v < M \tag{23}$$

with an absorbing boundary condition at $u = L$. The assumption that $\mathcal{O}_q$ is a primary conformal operator[10] allows us to relate its expectation value on the cylinder to that in the disk,

$$\langle \mathcal{O}_q(w)\rangle = \left|\frac{dz}{dw}\right|^{x_q^b}\langle \mathcal{O}_q(z)\rangle \sim \left(\frac{2\pi}{M}\right)^{x_q^b}\exp\left[-\frac{2\pi}{M}x_q^b(L-u)\right]. \tag{24}$$

This immediately gives the moments of the LDOS in the cylinder

$$\overline{[\rho(w)]^q} \sim \exp\left[-\frac{2\pi}{M}x_q^b(L-u)\right]. \tag{25}$$

From the exponential decay[31] of the moment $\overline{[\rho(w)]^q}$ away from the end of the semi-infinite cylinder in Eq. (25), for sufficiently small positive values of q, we identify the "q-dependent localization length" $\xi_p(q)$ in the cylinder geometry as

$$\xi_p(q) = \frac{M}{2\pi x_q^b}. \tag{26}$$

(Here "p" denotes again the "periodic" BCs of the cylinder.) The typical Q1D localization length ξ_p in cylinder geometry is read off from the typical exponential decay of the LDOS away from the end of the semi-infinite cylinder,

$$\overline{\ln \rho(w)} = -\frac{|L-u|}{\xi_p} + \cdots. \tag{27}$$

Expanding again Eq. (25) in q about $q=0$ yields

$$\frac{M}{\xi_p} = 2\pi\left.\frac{dx_q^b}{dq}\right|_{q=0} = 2\pi(\alpha_0^b - 2 + x_\rho), \tag{28}$$

where we have used Eq. (21). This is our previously mentioned result, Eq. (6), which generalizes Eq. (4) to all symmetry classes, including those with critical DOS.

In Sec. III D we numerically verify Eq. (6) for the spin quantum-Hall effect (symmetry class C) by computing numerically the FSS amplitude $\Lambda_p = 2\xi_p/M$ of the typical Q1D localization length ξ_p in cylinder geometry; according to our above-obtained result (28) this quantity is predicted to equal

$$\Lambda_p = \frac{1}{\pi(\alpha_0^b - 2 + x_\rho)} \tag{29}$$

with $x_\rho = 1/4$.

B. Finite-size scaling in strip geometry and surface (boundary) multifractal exponents

We now apply the same arguments to discuss finite-size scaling in the presence of open (reflecting) BCs in the transverse direction (strip geometry).

For this purpose we first consider the operator $\mathcal{O}_q$ placed close to the origin in the interior of the half disk $|z| \le R$, $\text{Im } z \ge 0$. The boundary of the system on the real axis is assumed reflecting, and the rest is attached to a metallic lead, as in the previous section. In this situation the expectation value of $\mathcal{O}_q(z)$ for $|z| \ll R$ is given by[32]

$$\langle \mathcal{O}_q(z)\rangle \sim R^{-x_q^s}, \tag{30}$$

where the boundary scaling dimension x_q^s (the superscript s stands for "surface") is typically different from the bulk dimension x_q^b. In analogy with Eq. (16) we now have, upon making again use of Eq. (13),

$$\overline{|\psi(z)|^{2q}} \sim R^{-2q - x_q^s + qx_\rho}, \tag{31}$$

where the same exponent x_ρ (a bulk exponent) enters through the global DOS. Note that Eq. (31) still implies $x_0^s = 0$ but now, in the boundary case, there is no restriction on x_1^s [in contrast to the bulk case: see Eq. (16) and the subsequent text]. Also, in complete analogy to the bulk case, the exponent of R in Eq. (31) must be a monotonic function of q. Upon expanding both sides of Eq. (31) in q about $q=0$, one

TABLE II. A list of parameters obtained or used in the FSS analysis for the scaling functions defined in Eqs. (41) and (57). Here Λ_c, ν, and y are obtained through fitting. N_d and N_p denote the numbers of data points and fitting parameters used in the fitting procedure, respectively. The fitting functions are truncated at the orders P and Q. χ^2 and g denote the values of chi squared and the goodness of fit probability, respectively.

System	BCs	Scaling function	Λ_c	ν	y	N_d	N_p	P	Q	χ^2	g
Symplectic (M-I)	Reflecting	Eq. (41)	1.50 ± 0.01	2.79 ± 0.03	-1.03 ± 0.03	85	9	2	2	86.2	0.2
Symplectic (M-QSH)	Reflecting	Eq. (41)	7.20 ± 0.01		-0.81 ± 0.08	8	3	0	0	7.2	0.2
IQH	Reflecting	Eq. (41)	1.624 ± 0.002	2.55 ± 0.01	-1.29 ± 0.04	134	6	3	2	144.0	0.2
SQH in class C	Periodic	Eq. (57)	0.8189 ± 0.0004	1.335 ± 0.016	-0.94 ± 0.01	73	8	2	2	56.2	0.7
SQH in class C	Reflecting	Eq. (41)	1.101 ± 0.002	1.335 ± 0.005	-1.05 ± 0.02	93	9	3	2	86.1	0.4

obtains the scaling exponent α_0^s of the typical wave-function amplitude *at the boundary*,

$$\overline{\ln|\psi(z)|^2} \sim -\alpha_0^s \ln R, \tag{32}$$

where now

$$\alpha_0^s = 2 - x_\rho + \left.\frac{dx_q^s}{dq}\right|_{q=0}. \tag{33}$$

Next, in order to relate this to the strip geometry, we use the conformal transformation

$$w = \frac{M}{\pi}\ln z, \quad z = \exp\left(\frac{\pi}{M}w\right), \tag{34}$$

which maps the half disk to a semi-infinite strip of width M in the w plane

$$w = u + iv, \quad u \le L \equiv \frac{M}{\pi}\ln R, \quad 0 \le v \le M. \tag{35}$$

The expectation value on the strip now follows again since $\mathcal{O}_q$, as a primary[10] conformal operator, transforms simply under conformal transformations,

$$\langle \mathcal{O}_q(w)\rangle = \left|\frac{dz}{dw}\right|^{x_q^s}\langle \mathcal{O}_q(z)\rangle \sim \left(\frac{\pi}{M}\right)^{x_q^s}\exp\left[-\frac{\pi}{M}x_q^s(L-u)\right]. \tag{36}$$

From this we obtain the exponential decay of the moments of the LDOS away from one end of the strip,

$$\overline{[\rho(w)]^q} \sim \exp\left[-\frac{\pi}{M}x_q^s(L-u)\right]. \tag{37}$$

As in the bulk case, the exponential decay[31] of the right-hand side in Eq. (37), for sufficiently small positive values of q, gives the "q-dependent Q1D localization length" along the strip

$$\xi_o(q) = \frac{M}{\pi x_q^s}. \tag{38}$$

As before, the typical Q1D localization length ξ_o in strip geometry is obtained by expanding both sides of Eq. (37) in q about $q=0$,

$$\frac{M}{\xi_o} = \pi\left.\frac{dx_q^s}{dq}\right|_{q=0} = \pi(\alpha_0^s - 2 + x_\rho), \tag{39}$$

where we have used Eq. (33). This is our previously announced result from Eq. (7).

In subsequent sections we verify Eq. (7) for various LD transitions by computing numerically the FSS amplitude $\Lambda_o = 2\xi_o/M$ of the Q1D typical correlation length ξ_o on the strip (o=open, reflecting BCs) which, according to our result, is predicted to be equal to

$$\Lambda_o = \frac{2}{\pi(\alpha_0^s - 2 + x_\rho)}. \tag{40}$$

III. NUMERICAL RESULTS

In this section we present the results of our numerical simulations supporting Eqs. (29) and (40). For convenience, we have gathered all the relevant fitting parameters and other numerical data in a single Table II.

In this section we have to distinguish off-critical and critical values of the Q1D localization lengths, ξ and ξ_c, and the corresponding FSS amplitudes, Λ and Λ_c (for both periodic and open BCs). All ξ and Λ that have appeared in the previous sections denoted values at the critical point.

A. Spin-orbit (symplectic) symmetry class

To compute the localization length at the LD transition in the symplectic class, we employed the so-called SU(2) model,[33] a tight-binding model on the square lattice, with random on-site disorder and fully random SU(2) hopping.

1. Localization length (strip geometry)

We obtained the typical localization length from the smallest Lyapunov exponent of transfer matrices for very long Q1D lattices. We imposed hard-wall, i.e., reflecting BCs in the transverse direction and hence our Q1D samples had strip geometry. Our systems had a maximum size $M=128$ in the transverse direction. Figure 1(a) shows the FSS amplitude $\Lambda_o = 2\xi_o/M$ of the typical Q1D localization length as a function of the on-site disorder strength W for various system sizes M and at fixed energy $E=0$ (band center). The curves for the various system sizes intersect at different points re-

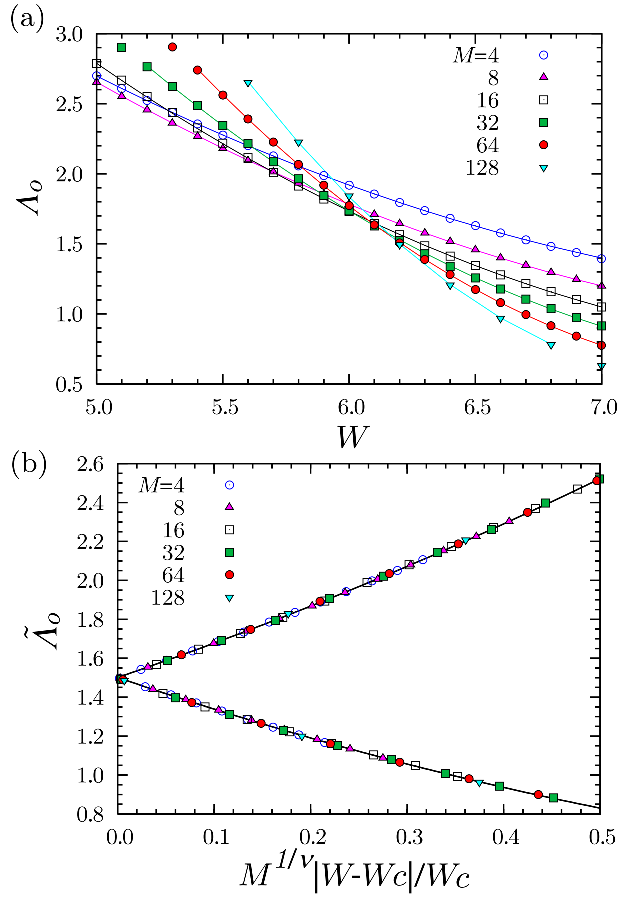

FIG. 1. (Color online) (a) Dependence of Λ_o on W at $E=0$ for various values of M. $\tilde{\Lambda}_o$ at $E=0$. (b) Scaling plot of $\tilde{\Lambda}_o$ at $E=0$, see Eq. (43). The obtained parameters are $\Lambda_{o,c}=1.50\pm0.01$, $W_c=6.192\pm0.007$, $\nu=2.790\pm0.025$, $y=-1.026\pm0.03$, $a_1=-1.69\pm0.03$, $a_2=0.70\pm0.02$, $b_0=1.24\pm0.03$, $b_1=-2.36\pm0.08$, and $b_2=4.7\pm0.3$.

flecting large finite-size effects, in contrast to the case of periodic BCs.[33]

To determine the critical value of the FSS amplitude $\Lambda_{o,c}$, we performed a FSS analysis incorporating corrections to scaling arising from the leading irrelevant scaling variable.[34] Specifically, we took a scaling function for the FSS amplitude of the form $\Lambda=F(\chi M^{1/\nu},\zeta M^{y})$, where χ is the relevant scaling variable, and ζ is the leading irrelevant scaling variable whose scaling exponent $y<0$. The exponent ν characterizes the divergence of the 2D localization length ξ upon approaching the LD transition point, $\xi\sim\chi^{-\nu}$. We expanded the scaling function around the critical point $W=W_c$, setting $\chi=(W-W_c)/W_c$,

$$\Lambda_o=\Lambda_{o,c}+\sum_{p=1}^{P}a_p(\chi M^{1/\nu})^p+M^y\sum_{q=0}^{Q}b_q(\chi M^{1/\nu})^q. \quad (41)$$

We fitted the numerical data to Eq. (41) with $P=Q=2$ by taking W_c, a_p, b_q, ν, and y as fitting parameters. We obtained

$$W_c=6.192\pm0.007,\quad \Lambda_{o,c}=1.50\pm0.01,$$

$$\nu=2.79\pm0.03,\quad y=-1.03\pm0.03. \quad (42)$$

The details of the fitting are summarized in Table II.

These results are in good agreement with those obtained by Asada *et al.*[33] for the SU(2) model with periodic BCs: $W_c=6.199\pm0.003$ and $\nu=2.75\pm0.04$ at $E=0$. The good quality of the fit can be seen from the scaling collapse, shown in Fig. 1(b), of the data for the corrected FSS amplitude $\tilde{\Lambda}_o$ defined by

$$\tilde{\Lambda}_o=\Lambda_o-M^y\sum_{q=0}^{Q}b_q(\chi M^{1/\nu})^q. \quad (43)$$

2. Surface multifractal exponent α_0^s

In our previous publication[13] we reported the value $\alpha_0^s=2.417\pm0.002$ for the surface exponent, which was obtained from numerical simulations on $L\times L$ lattices of system sizes up to $L=120$. We performed averaging over more than 6×10^4 disorder realizations. The lattices had periodic BC imposed in one of the two directions but open BC in the other direction, so our system had the geometry of a finite cylinder. Here we update the value for α_0^s reported in our previous work.[13] We use larger system sizes up to $L=180$, and average over up to 10^5 disorder realizations.

The surface exponent α_0^s was obtained from the system size dependence of the wave-function amplitude in the vicinity of the boundary, according to

$$\langle\langle\ln|\psi(x)|^2\rangle\rangle\sim-\alpha_0^s\ln L+c. \quad (44)$$

Here $x=\mathcal{O}(L^0)$, $L\gg1$, and c is a constant of order L^0. The double angular brackets represent both ensemble average and spatial average along the boundary of the cylinder in each disorder realization. First we tried a linear fitting to Eq. (44) of our numerical data for the left-hand side of Eq. (44), using system sizes $24\leq L\leq180$, with two fitting parameters α_0^s and c. This resulted in the value

$$\alpha_0^s=2.4195\pm0.0013. \quad (45)$$

Substitution of this value into Eq. (40) gave

$$\Lambda_{o,c}=1.518\pm0.005. \quad (46)$$

This analysis, however, ignored corrections from irrelevant scaling variables and was not quite correct since we now know from the previous section that such corrections are appreciable for the FSS amplitude Λ for open BC. We therefore reanalyzed the data, assuming scaling with corrections from the leading irrelevant variable.[18] We define

$$A(x):=-\frac{\langle\langle\ln|\psi(x)|^2\rangle\rangle}{\ln L}\sim\alpha_0^s+\frac{1}{\ln L}(c+c'L^y), \quad (47)$$

where we take $y=-1$, as suggested by Eq. (42). The fitting of the same data to Eq. (47) yielded

$$\alpha_0^s=2.429\pm0.006, \quad (48)$$

which leads to

$$\Lambda_{o,c} = 1.48 \pm 0.02 \tag{49}$$

with the help of Eq. (40). We see that the $\Lambda_{o,c}$ obtained from the transfer-matrix method (42) is consistent with these results. The value of α_0^s reported in Eq. (48) has larger error bars, which needs to be improved in future numerical work.

B. Metal-to-$\mathbb{Z}_2$-topological-insulator transition in quantum spin Hall systems

The $\mathbb{Z}_2$ topological insulator is a time-reversal invariant topological insulator in two dimensions, which possesses a topologically protected Kramers pair of extended edge states at its boundaries.[35] The $\mathbb{Z}_2$ topological insulating states can be realized in materials with strong spin-orbit interactions, as evidenced by recent experiments on HgTe/(Hg,Cd)Te quantum wells.[36] In the presence of disorder, this system undergoes a two-dimensional metal-insulator transition from a $\mathbb{Z}_2$ topological insulator to a metal, as one changes the Fermi energy. On symmetry grounds, this LD transition is expected to belong to the spin-orbit (symplectic) symmetry class.[37] Indeed, the critical exponent ν for the diverging localization length (a bulk property) at the metal-to-$\mathbb{Z}_2$-topological-insulator transition is found to agree with the value obtained for the SU(2) model,[37] which describes the metal-to-(ordinary) insulator transition in this symmetry class. Similar agreement is found for the multifractal exponents for critical wave functions in the bulk.[38] However, the multifractal exponents characterizing wave-function amplitudes at the sample *boundary* turn out to be different at the two metal-insulator transitions.

Here we show that, at the metal-to-$\mathbb{Z}_2$-topological-insulator transition, the FSS amplitude $\Lambda_{o,c}$ [Eq. (8)] for the typical Q1D correlation length in strip geometry, is related by conformal invariance to the boundary multifractal exponent α_0^s at the same transition.

1. Localization length (strip geometry)

To compute the localization length at the metal-to-$\mathbb{Z}_2$-topological-insulator transition, we employed the quantum spin-Hall network model.[37,38] An important parameter in this network model is the one controlling the probability of tunneling at the nodes of the network, which we denote by X. The numerical results shown below were obtained at the critical point $X_c=0.971$ with fully random SU(2) spin-rotation symmetry on each link.[38] Figure 2 shows the dependence of the FSS amplitude $\Lambda_o(M) \coloneqq 2\xi_o(M)/M$ of the typical Q1D localization length $\xi_o(M)$ on a strip of width M ($M=8,10,12,16,24,32,48,64$). Here M is the number of nodes of the network model in the transverse direction across the Q1D strip. This corresponds to transfer matrices of size $4M\times 4M$. In order to find the critical value $\Lambda_{o,c}$ of the FSS amplitude Λ_o in the large M limit, we assumed that Λ_o at $X=X_c$ has a power-law finite-size correction due to a leading irrelevant variable with dimension $y<0$

$$\Lambda_o(X = X_c) = \Lambda_{o,c} + b_0 M^y. \tag{50}$$

Fitting the data to this form (see Fig. 2), we obtained

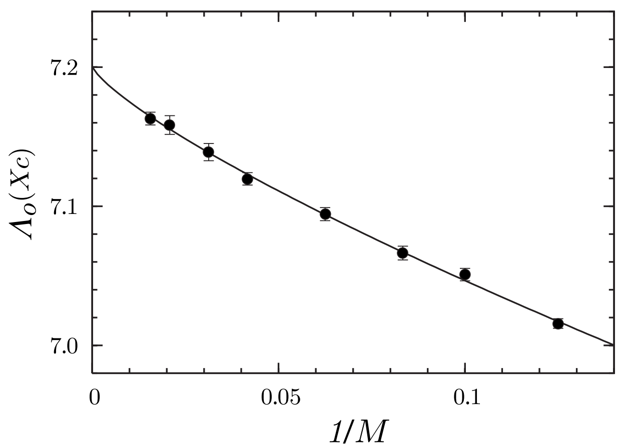

FIG. 2. M dependence of Λ_o at the metal-to-topological quantum spin-Hall insulator transition. The solid curve is a fit to Eq. (50) with $\Lambda_{o,c}=7.20\pm 0.01$, $y=-0.81\pm 0.08$, and $b_0=-1.0\pm 0.1$.

$$\Lambda_{o,c} = 7.20 \pm 0.01 \tag{51}$$

with $y=-0.81\pm 0.08$ and $b_0=-1.0\pm 0.1$. The details of the fitting are summarized in Table II.

2. Surface multifractal exponent α_0^s

The surface multifractal exponent at the metal-to-$\mathbb{Z}_2$-topological-insulator transition was obtained in Ref. 38. By using larger system sizes this value was recently improved in Ref. 39 to

$$\alpha_0^s = 2.091 \pm 0.002. \tag{52}$$

Substituting the improved value into Eq. (40) yields the FSS amplitude

$$\Lambda_{o,c} = 7.00 \pm 0.15. \tag{53}$$

This value is consistent with Eq. (51). The larger error bar in Eq. (53) results from the fact that the denominator in Eq. (40) (with $x_\rho=0$) contains $\alpha_0^s-2=0.091\pm 0.002$. Neither of the numerical analyses in Refs. 38 and 39, used to obtain Eq. (52), included effects of the leading irrelevant variable, in contrast to Eq. (51). These effects may influence the value of α_0^s and possibly result in better agreement with Eq. (51).

C. Plateau transition in the integer quantum-Hall effect

To compute the localization length ξ_o and the surface multifractal exponent α_0^s at the plateau transition in the IQH effect, we employed the Chalker-Coddington network model[40,41] in strip geometry with M nodes in the transverse direction across the strip. This corresponds to transfer matrices of size $2M\times 2M$. The plateau transition is reached by tuning a parameter θ which controls the tunneling probability at the nodes of the network model. For this model the critical value θ_c is known exactly.

1. Localization length (strip geometry)

The typical localization length ξ_o in Q1D strip geometry was computed numerically from the smallest Lyapunov ex-

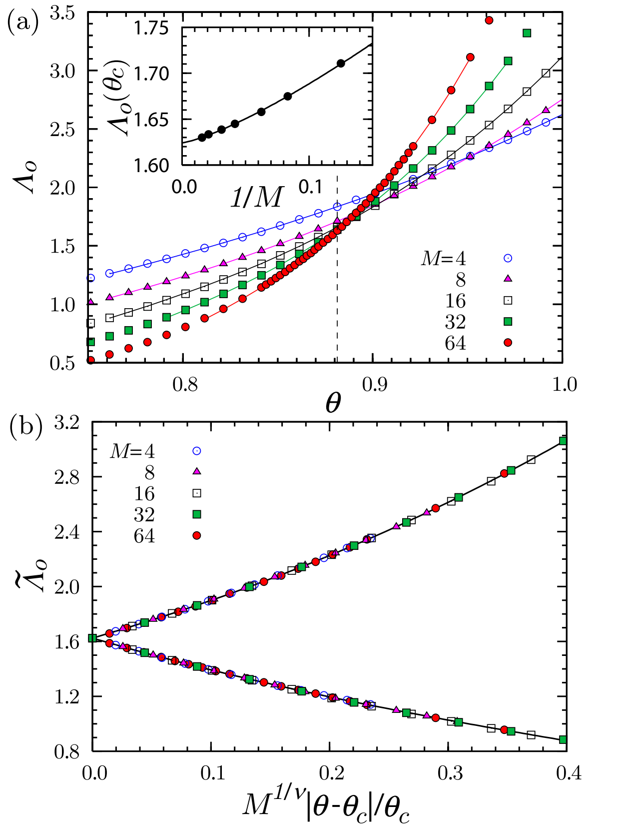

FIG. 3. (Color online) (a) Dependence of Λ_o on the node parameter θ in the Chalker-Coddington model of the strip geometry. The vertical dashed line indicates the critical point $\theta=\theta_c$. Inset: M dependence of Λ_o at $\theta=\theta_c$; the solid curve is a fit to Eq. (50). (b) Scaling plot from FSS analysis including corrections from the leading irrelevant scaling variable. The parameters used for the plot are $\nu=2.55\pm0.01$, $a_1=2.518\pm0.016$, $a_2=2.179\pm0.027$, $a_3=1.393\pm0.051$, $b_0=1.26\pm0.7$, $b_1=2.016\pm0.086$, and $b_2=-0.73\pm0.26$.

ponent of the transfer matrices. The largest system size (the number of network model nodes in the transverse direction) that we studied, was $M=64$. Figure 3(a) shows the FSS amplitude $\Lambda_o=2\xi_o/M$ of the typical localization length as a function of the network model tunneling parameter θ for various transverse system sizes M.[40] For $\theta>\theta_c$ the network model is in the quantum-Hall phase.[42] As seen from Fig. 3, the crossing point of the curves moves towards $\theta=\theta_c$ as M increases, indicating the presence of finite-size corrections. To find the critical value of the FSS amplitude Λ_o of the typical Q1D correlation length in the large M limit, we fitted the data to Eq. (50) [see the inset of Fig. 3(a)], to obtain

$$\Lambda_{o,c}=1.624\pm0.002, \tag{54}$$

$y=-1.29\pm0.04$, and $b_0=1.26\pm0.7$. The details of the fitting are summarized in Table II. Figure 3(b) shows the data collapse from the FSS analysis using Eqs. (41) and (43) with $\chi=(\theta-\theta_c)/\theta_c$ and the values of $\Lambda_{o,c}$, y, and b_0 obtained above. This FSS analysis also yielded $\nu=2.55\pm0.01$ for the critical exponent of the diverging (2D bulk) localization

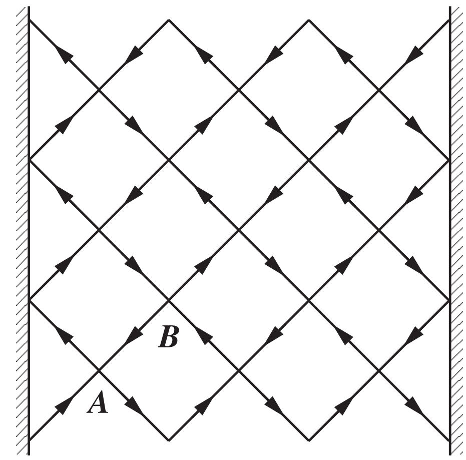

FIG. 4. The Chalker-Coddington network model on a cylinder. In the notation of Sec. III C 2 $L=3$ on this figure. There are $4L^2=36$ links and the unitary evolution operator U is a 36×36 matrix.

length, which is close to the value obtained in a recent large-scale numerical study, $\nu=2.593\pm0.006$.[43]

2. Surface multifractal exponent α_0^s

The surface multifractal exponent α_0^s at the plateau transition was recently obtained by the present authors[44] and by Evers *et al.*[45] It was found in these works that the multifractal analysis for the Chalker-Coddington model suffers from large finite-size corrections. To reduce these corrections, we have used, in the multifractal scaling analysis in Ref. 44, numerical data obtained only for large system sizes. Here we used an alternative approach by taking into account corrections to scaling arising from a leading irrelevant scaling variable using Eq. (47).

The geometry of the Chalker-Coddington network model that we used is shown in Fig. 4. There are two types of nodes forming two sublattices (denoted A and B in the figure), such that the A sublattice has the size $L\times L$ ($L=3$ in the figure). The links of the network form zigzag-shaped rows and columns; there are $2L$ such rows and $2L$ such columns so that the total number of links is $4L^2$. Integer x and y coordinates are assigned to the centers of links. We imposed periodic BC in the vertical y direction and reflecting BC in the horizontal x direction. The links in the first and the last columns at $x=1$ and $x=2L$ are called the edge links. The discrete time evolution of wave functions defined on links of the network model is governed by a unitary evolution operator U for one discrete time step, which is determined by the scattering S matrices at the nodes of the network model.[46] In our case this operator is a $4L^2\times4L^2$ unitary matrix. For each disorder realization, we obtained one critical wave function that is the eigenvector of U at $\theta=\theta_c$ and whose eigenvalue is closest to unity among all the eigenvectors. The largest system size we studied was $L=180$, and the disorder average was taken over 3×10^5 realizations for $L\leq60$, over 5×10^5 realizations for $L=80$, and over 2×10^5 realizations for $L=120,180$.

Figure 5(a) shows the x dependence of $\langle\langle\ln|\psi(x)|^2\rangle\rangle$, where the double angular brackets stand for both the average over disorder realizations and the spatial average along the

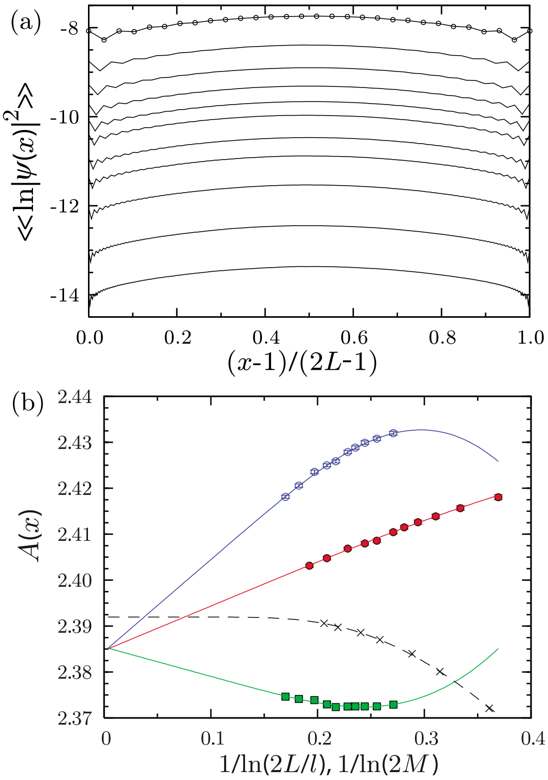

FIG. 5. (Color online) (a) Spatial dependence of logarithm of probability density $\langle\langle \ln|\psi(x)|^2\rangle\rangle$. The system size is changed as $L=15$, 20, 25, 30, 35, 40, 50, 60, 80, 120, and 180 from the top to the bottom. (b) Dependence of $A(x) := -\langle\langle \ln|\psi(x)|^2\rangle\rangle/\ln L$ on the effective system size L/l at $x=1$ (squares, $l=1$), 2 (open circles, $l=1$), and at edge plaquettes with coarse graining (filled circles, $l=2$), where l is the (linear) size of boxes used to define the coarse-grained wave-function probabilities. The solid curves are the fits to Eq. (47). Also shown by crosses is the dependence of $2[1+1/\pi\Lambda(\theta=\theta_c)]$ on the width M and its fit (dashed curve) to Eq. (50).

periodic y direction. We clearly observe in Fig. 5(a) Friedel-type oscillations near the edges of the cylinder, which become less pronounced as L is increased. [Such oscillations are absent in the SU(2) model discussed in the previous section.] Figure 5(b) shows how $A(x) = -\langle\langle \ln|\psi(x)|^2\rangle\rangle/\ln L$ approaches a constant value with increasing L at the left boundary ($x=1,2$). The solid curves show the fitting of $A(x)$ to Eq. (47) at $x=1$ (squares) and $x=2$ (open circles). To minimize the corrections coming from the Friedel-type oscillations, we defined the coarse-grained wave-function amplitude on each plaquette and calculated the corresponding A for the plaquettes along the edge (shown as filled circles). Fitting this coarse-grained data to Eq. (47) with $y=-1.29$ obtained in Sec. III C 1 yielded

$$\alpha_0^s = 2.385 \pm 0.003, \tag{55}$$

where the error bars reflect only statistical errors. This result is consistent with that of Ref. 44 ($\alpha_0^s=2.386\pm0.004$). Figure 5(b) shows that fitting of $A(x=1)$ and $A(x=2)$ gives similar values of α_0^s. Substituting Eq. (55) into Eq. (40) yields

$$\Lambda_{o,c} = 1.654 \pm 0.013, \tag{56}$$

which should be compared with $\Lambda_{o,c}=1.624\pm0.002$ [Eq. (54)] obtained from the transfer-matrix calculation. As we see in Fig. 5(b), finite-size corrections to A and Λ_o are still quite large at $L=180$. This makes the extrapolation of these quantities to $L\to\infty$ difficult; we cannot exclude the possibility of having systematic errors in addition to the statistical errors included in Eqs. (54) and (56). Given the presence of this uncertainty, we conclude that our numerical results are consistent with Eqs. (7) and (40).

D. Spin quantum-Hall plateau transition of BdG quasiparticles in symmetry class C

In this section we discuss the verification of Eqs. (6) and (7) for symmetry class C, which is known to possess a vanishing critical DOS ($x_\rho>0$). In our simulations we used an appropriate generalization of the Chalker-Coddington network model,[47] which we refer to as the class C network model. This model has a control parameter ϵ (in the notation of Ref. 47), and is critical at $\epsilon=0$. Exact values for critical exponents, $\nu=4/3$ and $x_\rho=1/4$, were obtained through mapping to classical percolation.[21,22] The exact values of the bulk[23] and surface[24] multifractal wave-function exponents $x_q^{b,s}$ are also known at $q=2,3$. However, exact results for the FSS amplitudes of the typical Q1D correlation lengths, $\Lambda_{p,c}$ and $\Lambda_{o,c}$, and the typical wave function scaling exponents $\alpha_0^{b,s}$ are not available.

1. Localization length (cylinder and strip geometries)

We numerically obtained the FSS amplitudes of the typical Q1D localization length of the class C network model for both cylinder and strip geometries. A previous numerical study[47] of FSS of the typical localization length in cylinder geometry did not report the value of $\Lambda_{p,c}$. Here we present results for the FSS amplitudes $\Lambda_{p,c}$ and $\Lambda_{o,c}$ corresponding to cylinder and strip geometries, respectively.

Cylinder geometry. Figure 6(a) shows the dependence of the FSS amplitude Λ_p of the typical Q1D correlation length on the parameter ϵ for various values of the transverse width M, obtained in cylinder geometry. The FSS amplitude Λ_p is symmetric about the critical point $\epsilon_c=0$ when periodic BCs are imposed. Hence in the FSS analysis we have to use an expansion in even powers of ϵ,

$$\Lambda_p = \Lambda_{p,c} + \sum_{p=1}^{P} a_{2p}(\epsilon M^{1/\nu})^{2p} + M^y \sum_{q=0}^{Q} b_{2q}(\epsilon M^{1/\nu})^{2q}. \tag{57}$$

The result of fitting of the data in Fig. 6(a) to Eq. (57) is shown in Fig. 6(b). The dependence of $\Lambda_p(\epsilon_c)$ on the width M at the critical point $\epsilon_c=0$ is plotted in Fig. 6(c). We obtained

$$\Lambda_{p,c} = 0.8189 \pm 0.0004 \tag{58}$$

and $\nu=1.335\pm0.016$. The details of the fitting are summarized in Table II. The latter result is consistent with the exact value $\nu=4/3$, indicating good accuracy of our numerical results.

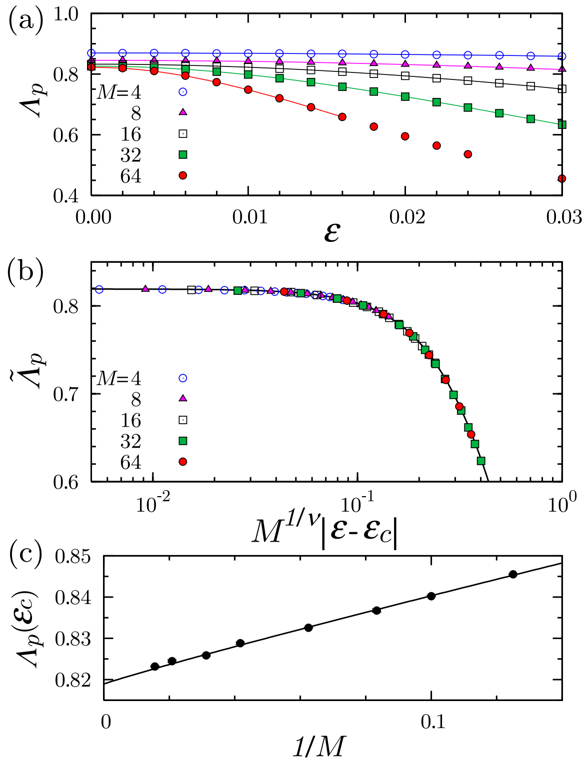

FIG. 6. (Color online) (a) Dependence of Λ_p on ϵ for several values of M in the class C network model of cylinder geometry. A critical point is known to be located at $\epsilon_c=0$. (b) Scaling plot of $\tilde{\Lambda}_p$, obtained after subtracting corrections to scaling from a leading irrelevant scaling variable. The parameters used for the plot are $\Lambda_{p,c}=0.8189\pm0.0004$, $\nu=1.335\pm0.016$, $y=-0.94\pm0.01$, $a_2=-1.66\pm0.10$, $a_4=3.64\pm0.33$, $b_0=0.185\pm0.003$, and $b_2=0.58\pm0.31$. (c) M dependence of Λ_p at $\epsilon=0$. The solid curve is a fit to Eq. (50).

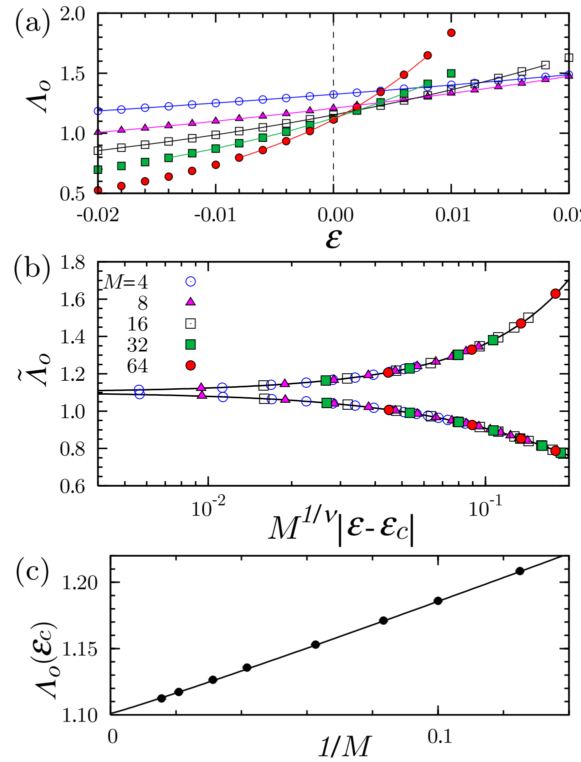

FIG. 7. (Color online) (a) Dependence of Λ_o on ϵ for several values of M in the class C network model of strip geometry. The critical point is located at $\epsilon_c=0$. (b) Scaling plot of $\tilde{\Lambda}_o$ from the FSS analysis with subtraction of corrections from a leading irrelevant scaling variable. The parameters used for the plot are $\Lambda_{o,c}=1.101\pm0.002$, $\nu=1.335\pm0.005$, $y=-1.05\pm0.02$, $a_1=2.225\pm0.024$, $a_2=3.221\pm0.083$, $a_3=2.91\pm0.20$ $b_0=0.960\pm0.015$, $b_1=1.846\pm0.095$, and $b_2=2.26\pm0.54$. (c) The M dependence of Λ_o at $\epsilon=0$. The solid curve is a fit to Eq. (50).

Strip geometry. Figure 7(a) shows the FSS amplitude of the typical Q1D correlation length in strip geometry. With reflecting BCs imposed in the transverse direction, the model possesses edge states for $\epsilon>0$ (the spin quantum-Hall phase, possessing topological order).[42] Since Λ_o is not a symmetric function of ϵ, we use the FSS function in Eq. (41). Figures 7(b) and 7(c) show the result of the FSS analysis and the width M dependence of the FSS amplitude $\Lambda_o(\epsilon_c)$ for the typical correlation length in the strip, respectively. From this analysis we obtained

$$\Lambda_{o,c} = 1.101 \pm 0.002 \tag{59}$$

and $\nu=1.335\pm0.005$. The details of the fitting are summarized in Table II.

2. Multifractal exponent α_0

The bulk and surface multifractal exponents α_0^b and α_0^s for the class C network model have been obtained numerically in Refs. 24 and 48,

$$\alpha_0^b \simeq 2.137, \quad \alpha_0^s \simeq 2.326. \tag{60}$$

Substitution of these values into Eqs. (29) and (40), respectively, with $x_\rho=1/4$ yields

$$\Lambda_{p,c} = 0.8225, \quad \Lambda_{o,c} = 1.105. \tag{61}$$

These values are consistent with the values presented in Eqs. (58) and (59) obtained by our FSS analysis.

IV. CONCLUSIONS

In this paper we have generalized the formula relating the multifractal exponent α_0 of the typical wave-function amplitude in a 2D sample to the FSS amplitude Λ_c of the typical localization length in a Q1D sample. Our generalization is twofold, resulting in Eqs. (6) and (7). Our Eq. (6) extends the relation to unconventional symmetry classes where the global density of states vanishes at criticality. Our Eq. (7) extends the relation to the case when the Q1D sample has strip geometry, instead of cylinder geometry which was always considered in earlier studies. In this case the multifractal exponent α_0^s describes the scaling of typical wave-function amplitude near the sample boundary.

We have verified generalized Eqs. (6) and (7) numerically for systems in four different universality classes: (a) the metal-to-insulator transition in the spin-orbit (symplectic) symmetry class, (b) the metal-to-($\mathbb{Z}_2$ topological insulator) transition also in the spin-orbit (symplectic) class, (c) the integer quantum-Hall plateau transition, and (d) the spin quantum-Hall plateau transition. Our numerical results are summarized in Tables I and II.

ACKNOWLEDGMENTS

We acknowledge helpful discussions with A. Mirlin, C. Mudry, and S. Ryu. This work was partly supported by the Next Generation Super Computing Project, Nanoscience Program from MEXT, Japan. Numerical calculations were performed on the RIKEN Super Combined Cluster System. H.O. is supported by JSPS. The work of A.F. was supported by a Grant-in-Aid for Scientific Research from MEXT and JSPS, Japan (No. 16GS0219 and No. 21540332). I.A.G. was partially supported by NSF under Grant No. DMR-0448820 and NSF MRSEC Grant No. DMR-0213745. The work of A.W.W.L. was supported in part by NSF under Grant No. DMR-0706140.

*Present address: FAS Center for Systems Biology, Harvard University, Cambridge, Massachusetts 02138, USA.

[1] P. W. Anderson, Phys. Rev. **109**, 1492 (1958).
[2] F. Wegner, Z. Phys. B **35**, 207 (1979).
[3] P. A. Lee and T. V. Ramakrishnan, Rev. Mod. Phys. **57**, 287 (1985).
[4] K. Efetov, *Supersymmetry in Disorder and Chaos* (Cambridge University Press, Cambridge, 1997).
[5] F. Evers and A. D. Mirlin, Rev. Mod. Phys. **80**, 1355 (2008).
[6] C. Castellani and L. Peliti, J. Phys. A **19**, L429 (1986).
[7] F. J. Wegner, Nucl. Phys. B **280**, 210 (1987).
[8] A. D. Mirlin, Phys. Rep. **326**, 259 (2000).
[9] M. Janssen, Int. J. Mod. Phys. B **8**, 943 (1994); Phys. Rep. **295**, 1 (1998).
[10] A. A. Belavin, A. M. Polyakov, and A. B. Zamolodchikov, Nucl. Phys. B **241**, 333 (1984).
[11] P. Di Francesco, P. Mathieu, and D. Sénéchal, *Conformal Field Theory* (Springer, New York, 1997).
[12] S. Hikami, A. I. Larkin, and Y. Nagaoka, Prog. Theor. Phys. **63**, 707 (1980); K. Jüngling and R. Oppermann, Z. Phys. B **38**, 93 (1980).
[13] H. Obuse, A. R. Subramaniam, A. Furusaki, I. A. Gruzberg, and A. W. W. Ludwig, Phys. Rev. Lett. **98**, 156802 (2007); Physica E **40**, 1404 (2008).
[14] J. L. Cardy, J. Phys. A **17**, L385 (1984).
[15] At any conventional nonrandom second-order phase transition in two dimensions, all scalar scaling operators which possess scaling dimensions smaller than two are examples of conformal primary operators.
[16] A. W. W. Ludwig, Nucl. Phys. B **330**, 639 (1990).
[17] A. Dohmen, P. Freche, and M. Janssen, Phys. Rev. Lett. **76**, 4207 (1996).
[18] F. Evers, A. Mildenberger, and A. D. Mirlin, Phys. Rev. B **64**, 241303(R) (2001).
[19] R. Merkt, M. Janssen, and B. Huckestein, Phys. Rev. B **58**, 4394 (1998).
[20] A. Mildenberger and F. Evers, Phys. Rev. B **75**, 041303(R) (2007).
[21] I. A. Gruzberg, A. W. W. Ludwig, and N. Read, Phys. Rev. Lett. **82**, 4524 (1999).
[22] E. J. Beamond, J. Cardy, and J. T. Chalker, Phys. Rev. B **65**, 214301 (2002).
[23] A. D. Mirlin, F. Evers, and A. Mildenberger, J. Phys. A **36**, 3255 (2003).
[24] A. R. Subramaniam, I. A. Gruzberg, A. W. W. Ludwig, F. Evers, A. Mildenberger, and A. D. Mirlin, Phys. Rev. Lett. **96**, 126802 (2006).
[25] M. R. Zirnbauer, J. Math. Phys. **37**, 4986 (1996); A. Altland and M. R. Zirnbauer, Phys. Rev. B **55**, 1142 (1997).
[26] Not to be confused with the "spin quantum-Hall" transition in symmetry class C, mentioned above.
[27] These assumptions have been numerically verified in Ref. 13 for one of the standard symmetry classes which possess a LD transition in 2D, namely, for the 2D metal-insulator transition in the spin-orbit (symplectic) class.
[28] Note that this boundary condition has nothing to do with the open (reflecting) boundary condition we consider in Sec. II B.
[29] In a supersymmetric sigma model arbitrary real moments of the local density of states can be obtained by exploiting the noncompact sector of the theory.
[30] See, e.g., T. C. Halsey, M. H. Jensen, L. P. Kadanoff, I. Procaccia, and B. I. Shraiman, Phys. Rev. A **33**, 1141 (1986).
[31] It is known (Ref. 5) that the exponents x_q^b are positive only within some range $0<q<q_*$. Outside this range $x_q^b<0$, which leads to LDOS moments $[\rho(w)]^q$ that are exponentially growing away from the cylinder boundary. This can be explained by the following argument. In cylinder geometry, the wave functions are localized, and the level broadening η created by the metallic lead attached at the edge $u=L$ is strongly coordinate dependent. Indeed, the overlap of a wavefunction localized at a point w away from the cylinder edge with the extended wave functions in the lead is exponentially small, which results in an escape rate, that is, a level broadening that is exponentially decaying away from the edge: $\eta(u) \propto e^{-(L-u)/\xi}$. Here ξ is the typical localization length. Thus, away from the edge, the profile of the LDOS (as a function of energy) consists of well-resolved narrow Lorentzian peaks [see Eq. (10)] of width of order $\eta(u)$ and height proportional to $1/\eta(u)$. Only within the range $0<q<q_*$ corresponding to $x_q^b>0$ are the moments of the LDOS determined by the minima of the LDOS profile [where the LDOS is proportional to $\eta(u)$]. For other values of q the dominant contribution to the moments of LDOS comes from the maxima in the LDOS profile. In the described situation the behavior of the moments of the wave functions is very different from that of the moments of the LDOS. However, we can directly relate the latter to the transmission through the cylinder from the metallic lead. Essentially, the transmission will be exponentially small away from the edge of the cylinder if the energy of the incoming wave (in the lead) corresponds to a minimum in the LDOS profile but will be of order one (it cannot be bigger) if the energy is in resonance with one of the broadened energy levels (that is, a peak in the LDOS profile).

[32] The dependence on z, which encodes the distance from the boundary, is suppressed here.

[33] Y. Asada, K. Slevin, and T. Ohtsuki, Phys. Rev. Lett. **89**, 256601 (2002); Phys. Rev. B **70**, 035115 (2004).

[34] K. Slevin and T. Ohtsuki, Phys. Rev. Lett. **82**, 669 (1999).

[35] C. L. Kane and E. J. Mele, Phys. Rev. Lett. **95**, 146802 (2005); **95**, 226801 (2005).

[36] M. König, S. Wiedmann, C. Brüne, A. Roth, H. Buhmann, L. W. Molenkamp, X.-L. Qi, and S.-C. Zhang, Science **318**, 766 (2007).

[37] H. Obuse, A. Furusaki, S. Ryu, and C. Mudry, Phys. Rev. B **76**, 075301 (2007).

[38] H. Obuse, A. Furusaki, S. Ryu, and C. Mudry, Phys. Rev. B **78**, 115301 (2008).

[39] S. Ryu, C. Mudry, H. Obuse, and A. Furusaki, New J. Phys. **12**, 065005 (2010).

[40] J. T. Chalker and P. D. Coddington, J. Phys. C **21**, 2665 (1988).

[41] B. Kramer, T. Ohtsuki, and S. Kettemann, Phys. Rep. **417**, 211 (2005).

[42] In this phase Λ_o increases with M, due to the presence of edge states, which increase the conductance (similar to the case of a metallic phase).

[43] K. Slevin and T. Ohtsuki, Phys. Rev. B **80**, 041304(R) (2009).

[44] H. Obuse, A. R. Subramaniam, A. Furusaki, I. A. Gruzberg, and A. W. W. Ludwig, Phys. Rev. Lett. **101**, 116802 (2008).

[45] F. Evers, A. Mildenberger, and A. D. Mirlin, Phys. Rev. Lett. **101**, 116803 (2008).

[46] R. Klesse and M. Metzler, Europhys. Lett. **32**, 229 (1995).

[47] V. Kagalovsky, B. Horovitz, Y. Avishai, and J. T. Chalker, Phys. Rev. Lett. **82**, 3516 (1999).

[48] F. Evers, A. Mildenberger, and A. D. Mirlin, Phys. Rev. B **67**, 041303(R) (2003).